ADVANCED FUNCTIONAL MATERIALS

www.afm-journal.de

Toward Stretchable Self-Powered Sensors Based on the Thermoelectric Response of PEDOT:PSS/Polyurethane Blends

*Prospero J. Taroni, Giovanni Santagiuliana, Kening Wan, Philip Calado, Manting Qiu, Han Zhang, Nicola M. Pugno, Matteo Palma, Natalie Stingelin-Stutzman, Martin Heeney, Oliver Fenwick, Mark Baxendale, and Emiliano Bilotti**

The development of new flexible and stretchable sensors addresses the demands of upcoming application fields like internet-of-things, soft robotics, and health/structure monitoring. However, finding a reliable and robust power source to operate these devices, particularly in off-the-grid, maintenance-free applications, still poses a great challenge. The exploitation of ubiquitous temperature gradients, as the source of energy, can become a practical solution, since the recent discovery of the outstanding thermoelectric properties of a conductive polymer, poly(3,4-ethylenedioxythiophene)-poly(styrenesulfonate) (PEDOT:PSS). Unfortunately the use of PEDOT:PSS is currently constrained by its brittleness and limited processability. Herein, PEDOT:PSS is blended with a commercial elastomeric polyurethane (Lycra), to obtain tough and processable self-standing films. A remarkable strain-at-break of ≈700% is achieved for blends with 90 wt% Lycra, after ethylene glycol treatment, without affecting the Seebeck voltage. For the first time the viability of these novel blends as stretchable self-powered sensors is demonstrated.

1. Introduction

The fast developing field of wearable electronics for autonomous monitoring is combining smart textile technology with state of the art wireless sensing communication, and it could soon experience exponential growth as new applications are being considered for fields such as internet-of-things, soft robotics, medicine, defence, advertising, fashion, and many others.[1–5] On the other hand, numerous challenges are still to be overcome, including the need for improved materials that are not only responsive to specific stimuli but can also conform to the objects monitored, for instance being flexible and stretchable, as well as durable.[6] Another important requirement is to make the sensors autonomous and self-powered, particularly desirable in off-grid,

P. J. Taroni, G. Santagiuliana, K. Wan, Dr. H. Zhang, Prof. N. M. Pugno, Dr. O. Fenwick, Dr. E. Bilotti
School of Engineering and Material Sciences
Queen Mary University of London
Mile End Road, E1 4NS London, UK
E-mail: e.bilotti@qmul.ac.uk

P. Calado
School of Physics
Imperial College London
London SW7 2AZ, UK

Dr. M. Baxendale, M. Qiu
School of Physics and Astronomy
Queen Mary University of London
Mile End Road, London E1 4NS, UK

Prof. N. M. Pugno
Laboratory of Bio-inspired & Graphene Nanomechanics
Department of Civil, Environmental and Mechanical Engineering
University of Trento
Via Mesiano 77, 38123 Trento, Italy

The ORCID identification number(s) for the author(s) of this article can be found under https://doi.org/10.1002/adfm.201704285.

DOI: 10.1002/adfm.201704285

Prof. N. M. Pugno
Ket-Lab
Edoardo Amaldi Foundation
Italian Space Agency
Via del Politecnico snc, 00133 Rome, Italy

Dr M. Palma
School of Biological and Chemical Sciences
Queen Mary University of London
Joseph Priestley building, Mile End Road, London E1 4NS, UK

Prof. N. Stingelin-Stutzman
School of Materials Sciences
Georgia Tech
771 Ferst Drive, J. Erskine Love Building, Atlanta GA 30332-0245, USA

Prof. M. Heeney
School of Chemistry and Centre of Plastic Electronics
Imperial College London
London SW7 2AZ, UK

maintenance-free conditions, where battery replacement is not practical, economical or feasible.[5] There have been different research strategies for finding sustainable, small scale energy harvesting systems to recharge batteries or to directly power sensor devices, with long lasting and reliable supplies. This has been demonstrated so far using triboelectric,[7–11] photovoltaic,[5,12] piezoelectric,[5,13,14] radiofrequency,[14] thermoelectric (TE) systems,[14–18] and others.[19–21] In the case of TE technology, conventional systems have been considered as a power source for integrated sensors of pressure,[22] corrosion,[23] heat flow,[24] vibration,[25] heart rate,[26] and other stimuli.[27–31] The utilization of conjugated polymers as the active component of a TE device is a relatively recent concept,[32–34] but it is rather attractive where flexibility is needed, enabling a new generation of novel, low-cost, low-powered wearable, or even remote, sensors. There are many desirable attributes driving the investigation of polymer TE materials, such as low toxicity, ubiquity, and abundance of constitutive elements, as well as ease in processing by various established coating or printing techniques. Poly(3,4-ethylenedioxythiophene)-poly(styrenesulfonate) (PEDOT:PSS) is at the centre of the effort to achieve thermoelectric power conversion efficiencies comparable to those of inorganic thermoelectric materials. In 2003, PEDOT was reported to have a dimensionless figure of merit (zT value) as high as 0.42.[35] This result is within close reach of the best commercial inorganic materials used for room temperature applications, such as bismuth telluride compounds, with zT value around 1.[36–38] Promising results were also obtained by combining PEDOT, or other conductive polymers (e.g., P3HT and PANi), with carbon nanotubes and other nanoparticles.[39–42] PEDOT was further studied as a *p*-type TE material,[43–53] and shown to be sensitive to stimuli like temperature and pressure.[54] However, a number of challenges still restrict its commercial exploitation, including low toughness and tear resistance, in addition to processing constraints, limited to film casting from water solution, while bulk (greater than tens of microns thick) processing is needed to fulfill current TE device design requirements.

Here we propose a novel strategy for overcoming the above limitations, consisting of blending PEDOT:PSS with a commercial polyurethane (Lycra), followed by post-treatment of the films with ethylene glycol (EG), a polar solvent known to improve the thermoelectric behaviour of PEDOT:PSS.[37] After a systematic study of blend composition, film morphology, as well as mechanical and TE characterization, a new set of materials were obtained. They are stretchable and tough, of relative low cost and potentially compatible with bulk industrial processing (e.g., extrusion, melt spinning), while maintaining the same Seebeck coefficient values as pure PEDOT:PSS. The sensing efficiency of these blends were then studied with the use of an external power source, where the resistance is determined and correlated with the changes in film geometry when responding to strain. Furthermore, with a temperature difference across the end of the film, the resultant thermovoltage was found to produce a measurable sensing signal which was used to detect changes in strain as well as ambient temperature and/or air flow. The results presented in this paper promise to be a viable solution for applications such as self-powered sensors.

2. Results and Discussion

In this study, freeze-dried PEDOT:PSS and the elastomeric Lycra yarn were separately dispersed in dimethyl sulfoxide (DMSO), then mixed together at different proportions, aiming at maximizing mechanical behavior and strain-sensing capabilities. Free-standing films were produced by drop casting onto glass substrates. Post-treatment was performed by immersing the films in an EG bath.

2.1. Mechanical Properties

The mechanical properties of the blend films have been studied using quasi-static tensile tests and presented in **Figure 1**a,b,

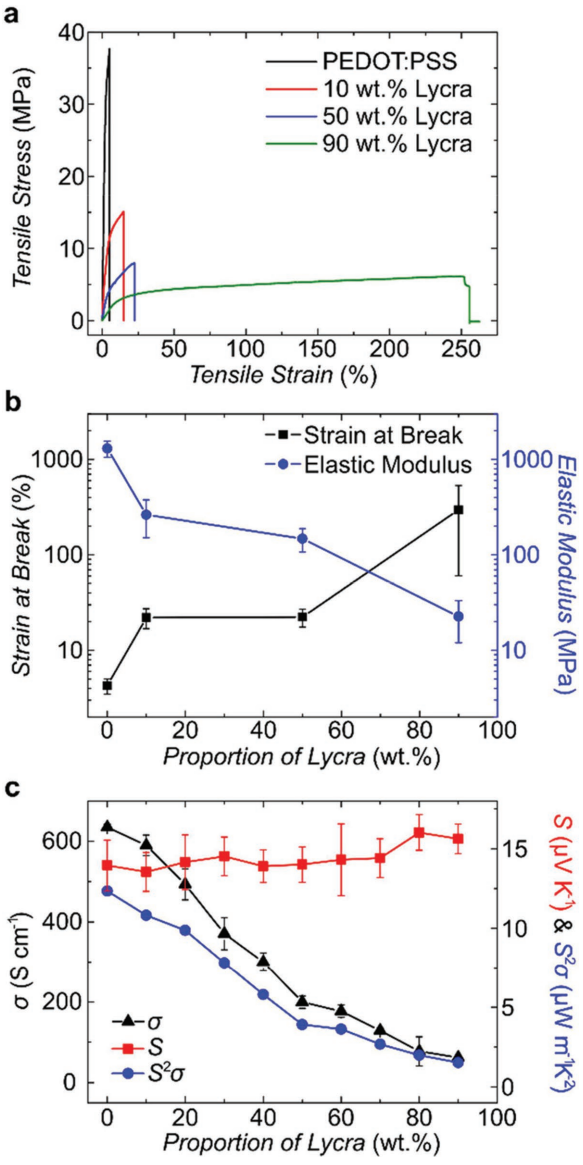

Figure 1. a) Stress vs strain behavior of PEDOT:PSS blends with various proportions of Lycra, b) elastic modulus and strain-at-break for the same blends, and c) electrical conductivity, Seebeck coefficient, and power factor of films of PEDOT:PSS blends with various proportions of Lycra (all graphical results are before EG treatment).

showing typical stress–strain responses as a function of Lycra content. The strain-at-break value increases with increased concentration of elastomer, from 4 ± 1% at 0 wt% Lycra (pure PEDOT:PSS) to 300 ± 230% at 90 wt%, while the elastic modulus is inversely correlated, going from 1300 ± 250 MPa for pure PEDOT:PSS to 23 ± 11 MPa at 90 wt% Lycra. Thus blending clearly improve the ductility of PEDOT:PSS. A rather large deviation in results for films with high elastomer content was observed. This is possibly due to microstructural inhomogeneity of films related to subtle variation in the casting temperature, which was demonstrated to significantly affect phase-segregation of the components (Section S1, Supporting Information).

Some of the samples containing 90 wt% Lycra were also immersed in an EG bath after casting. They exhibited outstanding improvements in elastic modulus and strain-at-break, with values of 75 ± 65 MPa and 700 ± 150%, respectively. These mechanical properties are unprecedented for a TE material, and closely approach the ones of neat elastomeric yarns (Section S2, Supporting Information).

2.2. Thermoelectric Properties

A simplified way to quantify the ability of a given material to generate useful thermoelectricity, is the measurement of the power factor (PF), expressed in Equation (1)

$$\mathrm{PF} = S^2 \times \sigma \tag{1}$$

where S is the Seebeck coefficient, the voltage difference generated by unit of temperature, and σ is the electrical conductivity. The power factor, electrical conductivity, and Seebeck coefficient of all the blends are presented in Figure 1c.

The electrical conductivity of the blended films decreases nearly linearly with increasing proportion of elastomer, from 635 ± 8 S cm^{-1} for unmodified PEDOT:PSS to 62 ± 4 S cm^{-1} for 90 wt% Lycra. These relatively high values can be explained by the effect of the chosen solvent (DMSO), which is known to improve the electrical conductivity of PEDOT:PSS.[55] Further improvements can be achieved if films are treated with an EG bath, giving up to 26% increase in electrical conductivity for composites containing 90 wt% Lycra, reaching an averaged value of 79 ± 5 S cm^{-1}. Indeed, EG treatment consistently resulted in improved conductivity, as summarized in Section S3 in the Supporting Information. EG has been previously shown to help controlling the film morphology through removal of excess insulating PSS.[48] The X-ray diffractograms presented in Section S4 in the Supporting Information confirm extraction of excess PSS from the film through a reduction of signal intensity for the peak at $2\theta \approx 18°$.

The Seebeck coefficient stayed relatively constant, invariant with the proportion of Lycra (Figure 1c). This is of great importance because blends with high proportions of elastomer will be able to produce a similar thermovoltage as neat PEDOT:PSS (useful for self-power capability), while gaining significant elasticity and toughness (as demonstrated in Section 2.1), Furthermore, the Seebeck coefficient of PEDOT:PSS is apparently not reduced by EG treatment (Section S5, Supporting Information).

As for the electrical conductivity, also the power factor follows a similar declining trend with increasing proportion of Lycra. Therefore, in this case, the electrical conductivity has a stronger influence than the Seebeck coefficient on PF.

2.3. Morphology

For a better understanding of the mechanical and thermoelectric properties presented in this paper, a systematic study of blend composition and film morphology was undertaken. Optical transmission studies of the films with varying composition revealed no evidence of any chemical reaction upon blending (Section S6, Supporting Information). The study of atomic force microscopy (AFM) imaging, in quantitative nanomechanical analysis mode, was used to investigate the morphology of the films, after EG treatment, shown in **Figure 2**. These images depict the relative elastic moduli of the film surfaces and clearly show the dispersion of Lycra-rich regions (low elastic modulus) into PEDOT:PSS-rich regions (high elastic modulus), with a continuous change in morphology between

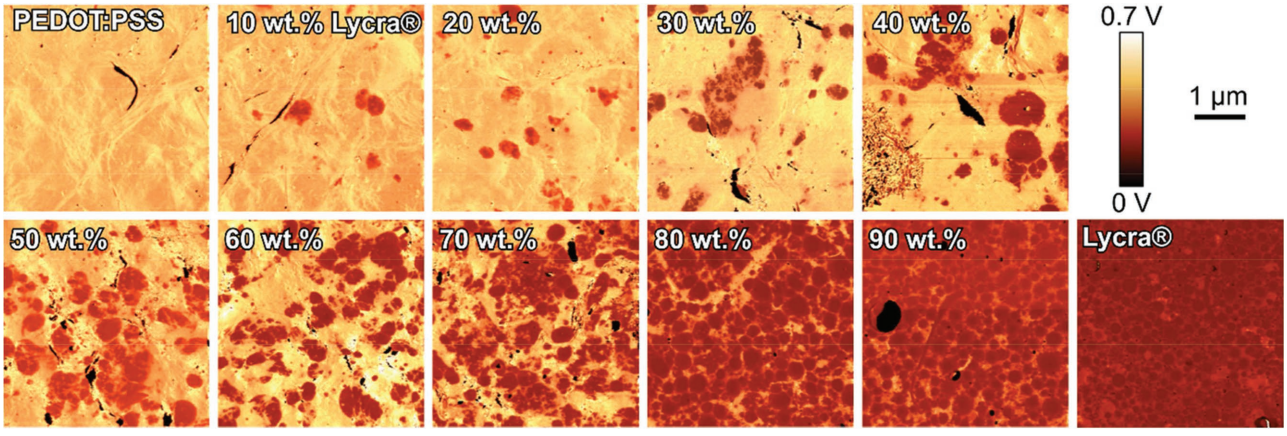

Figure 2. AFM images (4 × 4 µm) of the PEDOT:PSS/Lycra film surfaces obtained in nanomechanical analysis mode. The colourscale is an indicator of the voltage signal from the instrument, which is proportional to the elastic modulus. Lycra-rich regions appear dark (low elastic modulus) and PEDOT:PSS-rich regions appear bright (high elastic modulus).

the two pure materials. Nanomechanical imaging offers in this case an improved contrast as compared to topography-mode, owing to the significant difference in elastic modulus between the two polymers. Further studies of AFM imaging revealed the Lycra-rich regions to exhibit greater deformation, adhesion, and dissipation than PEDOT:PSS-rich regions (Section S7a, Supporting Information). A low degree of connectivity between domains, for films with less than 60 wt% Lycra, is also shown in Figure 2, which we would expect to have detrimental effects on elasticity and toughness, as the elastomer may not be forming a continuous network, leading to more brittle and rigid materials. Yet this is not what we observed in macroscopic tests. Since these are surface images, so we cannot rule out an extended Lycra component embedded within the film structure.

The study of topography-mode AFM imaging (Section S7b, Supporting Information) revealed a root mean square (rms) roughness of 540 nm for blended films of thickness ≈10 µm, which is more than an order of magnitude greater than that of commercial PEDOT:PSS cast from aqueous suspension. For the pure Lycra films, a value of 350 nm was found.

The top surface and cross-sectional area of the blended films, before and after EG treatment, were also studied by scanning electron microscopy (SEM), presented in Section S8 in the Supporting Information. A trend toward compact structure with increasing Lycra content is evident, which could explain the decrease in roughness observed by AFM. No distinct microstructural differentiation is apparent in the images of films before and after EG treatment. Some isolated PEDOT:PSS domains are visible in the cross-section of films with 90 wt% Lycra, although the conductive pathway may not be a sole result of these apparently discontinuous sites. As previously discussed in Section 2.1, it is possible that the components partly phase-segregate during casting of the films.

2.4. Externally Powered Strain Sensing

Sensitivity to strain was determined by a bespoke test set-up, in which the electrical resistance (R) is measured by passing a current from an external power supply through the sample while simultaneously subjecting it to a given strain profile. These tests were performed on films containing 90 wt% Lycra, previously subjected to EG treatment, owing to the high values of elasticity and electrical conductivity. As shown in **Figure 3**a,b, the modulation of resistance is up to 20% and 80% for strains of 10% and 50%, respectively, and this behavior can be

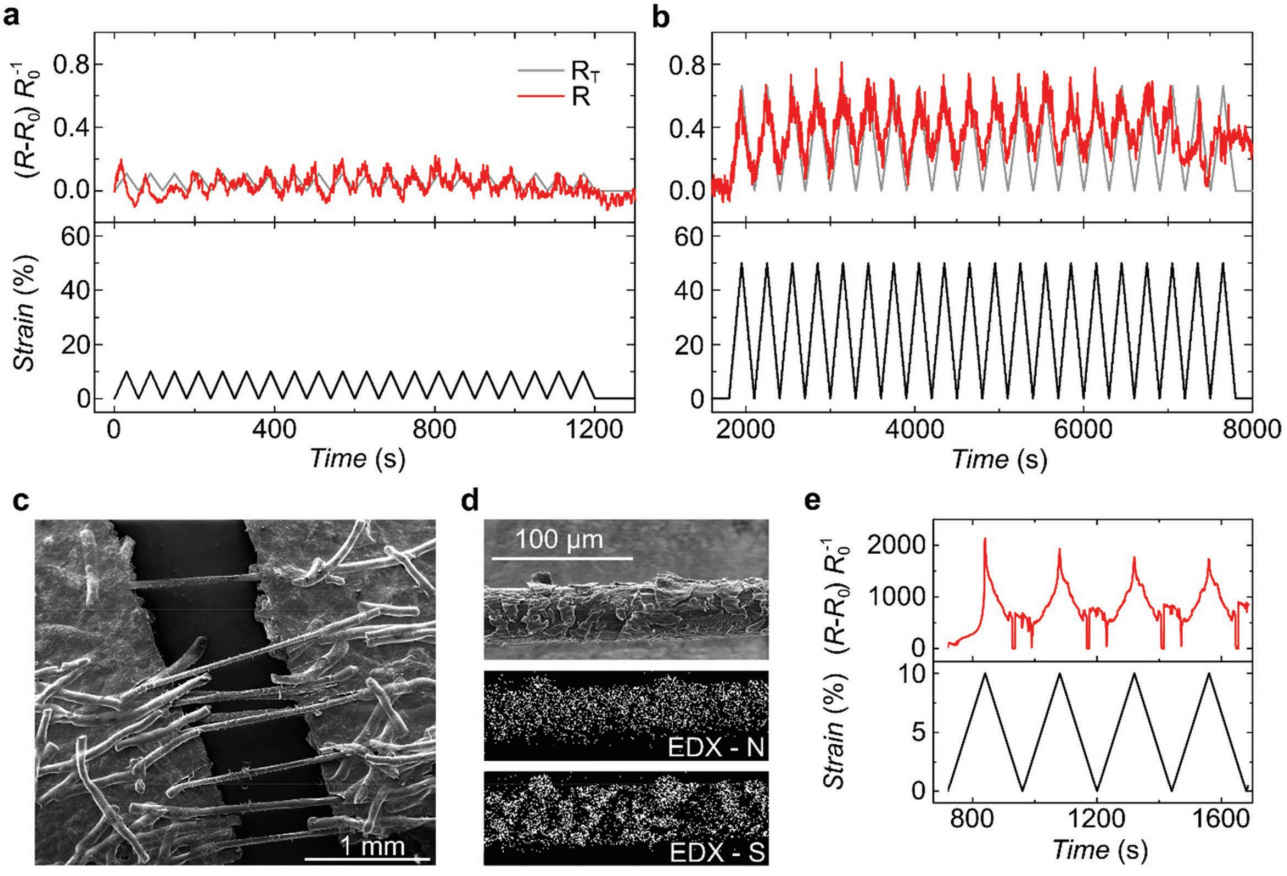

Figure 3. a) $(R–R_0)\ R_0^{-1}$ as a function of strain, where R_0 is the resistance at zero strain, for films of PEDOT:PSS blended with 90 wt% Latex previously subject to EG treatment, when 10% strain is applied, followed by 50% (Gauge factor ≈1 and 1.3, respectively). The theoretical resistance R_T is shown in red. b) SEM imaging of a cracked film surface of 50 wt% Lycra used for strain sensing, showing stretched bridging filaments, c,d) SEM and EDX of one stretched filament for detection of sulphur (from PEDOT:PSS) and nitrogen (from Lycra), e) plot of $(R–R_0)\ R_0^{-1}$ as a function of strain for this film, after cracking.

explained with a simple geometrical effect. By assuming incompressibility (Poisson ratio of 0.5),[56] and a constant resistivity, one can calculate the reduction of sample cross-sectional area for a given extension, and hence a theoretical resistance (R_T), (Section S9, Supporting Information). The variation of R with strain is very well predicted by this simple model. Nonetheless, for strains higher than 50%, the values of R are higher than R_T, indicating change in intrinsic resistivity may also be involved (Section S10, Supporting Information). This can be explained by a possible modification of the conductive network. At relatively high strains (>80%), the sample exhibited plastic deformation, with a permanent increased resistance.

A strategy to overcome this limitation, while increasing the strain sensitivity further still, can come from engineering the conductive network morphology. It has been noticed that some samples with lower elastomer content (50 wt% Lycra) and prepared from poorly dissolved Lycra presented some intact short filaments from the original yarn in the final composite film (Figure 3c). In these cases, the filaments indirectly control the morphology of the conductive network, in terms of excluding a volume in which PEDOT:PSS can be dispersed, but also in guiding its dispersion, which seems to preferentially coat the filaments (Figure 3d). Once the composite film cracks, after exceeding a threshold strain of ≈10%, filaments coated with PEDOT:PSS were still observed connecting the two extremities of the cracked sample (fibre bridging), bearing the load. The strain sensing tests for these samples show an interesting bimodal behavior. For strains lower than the threshold, the material is not sensitive, while for higher strain (after crack formation), the strain, sensitivity suddenly increases (with an outstanding Gauge Factor of ≈17 000–20 000 when 10% strain is applied). The strain, localised on the bridging filaments, determines the pathway for charge carrier transport (Figure 3e). Interestingly, this change in resistance is reversible, with the normalised resistance going back to initial values before cracking, when the strain decreases to zero. In future, we envisage the development of new materials inspired by these intriguing results, where, for instance, Lycra fibres are coated with PEDOT:PSS, which can then be used for conductive film reinforcement or as a sensing device on its own. Initial tests have already started with encouraging initial results (Section S11, Supporting Information).

2.5. Self-Powered Strain Sensing

To demonstrate the concept of a self-powered strain sensor based on the thermoelectric effect, a film containing 90 wt% Lycra was exposed to a constant temperature difference of 30 °C, while uniaxially deformed (**Figure 4**a). When the sample was series-connected to a 10 kΩ load resistor, a thermocurrent was induced by the Seebeck voltage. It is noted that the load resistance of 10 kΩ was selected to match the internal specimen resistance at high strains, hence maximizing the power output. However, the internal resistance does change with the applied strain (Section S10, Supporting Information). So, for a more efficient self-powered strain sensor, the load resistance should ideally be modulated with the strain. Nevertheless, Figure 4c demonstrates that large strains, above 80%, can clearly be sensed by a simultaneous change in voltage and current. In order to explain this, it is observed that the thermovoltage generated is assumed constant with strain (Section S12, Supporting Information), while the resistance of the sample varies. Hence the thermocurrent generated, passing through the external circuit, also varies. Considering the equivalent circuit in Figure 4b, the voltage measured across the load resistor is proportional to the load resistance only, and therefore it changes proportionally to the thermocurrent variation, in agreement with measurements presented in Figure 4c. But the self-powered sensor does not respond only to strain. In fact it shows sensitivity to other stimuli, for instance, ambient temperature and/or air currents (Section S13, Supporting Information).

It is noted that the sample in Figure 4, can harvest a power output of up to few nW (Section S14, Supporting Information) for a ΔT of 30 °C. Increasing the power output to the level of

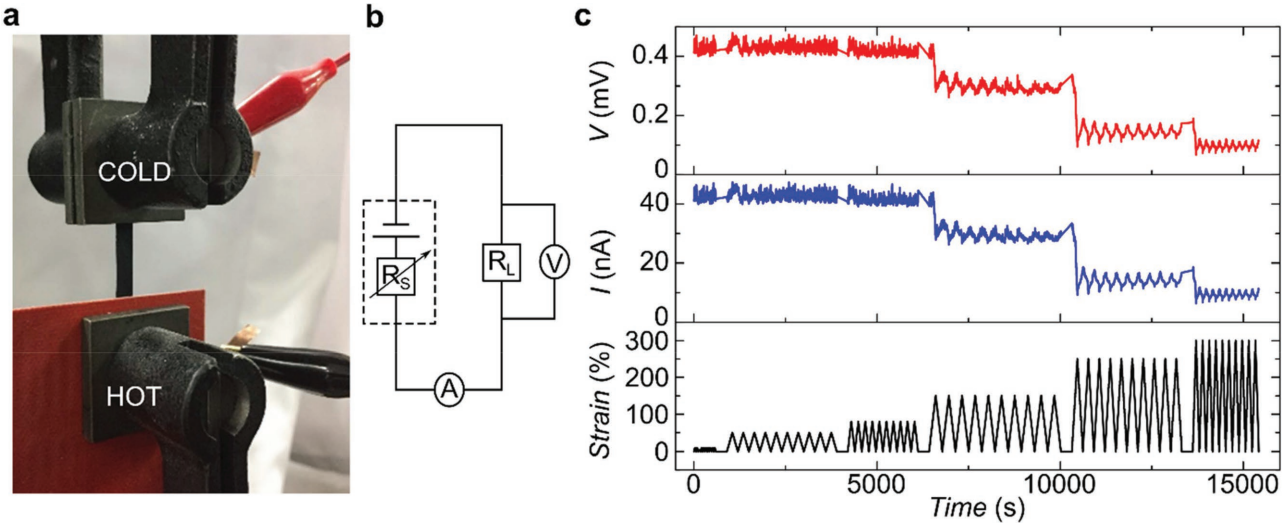

Figure 4. a) Experimental setup for the proof-of-concept of self-powered strain sensor measurements. b) The equivalent circuit for the film under test, the voltage source is the thermovoltage generated by the temperature difference across the ends of the sample, R_s is the internal resistance of the film and R_L is the external load resistance. c) The variation of voltage across and current through the load resistor with strain and time.

10–100 μW, necessary for an integrated self-powered system (including data trasmission for instance) can be achieved by: (i) increasing the temperature gradient, (ii) connecting our p-type TE material in series with a n-type one, to form a p–n junction, (iii) connecting many p-n junctions in series.

3. Conclusion

This work demonstrates a strategy to develop stretchable self-powered sensors, via blending an elastomeric polyurethane (Lycra) with the best current organic thermoelectric material, PEDOT:PSS. In doing so, the main technological constrains of PEDOT:PSS, namely brittleness, processability, and costs, have, at the same time, been overcome. An unprecedented strain at break of 700 ± 150% has been reached, for a blend containing 90 wt% Lycra, after EG bath, while maintaining high electrical conductivity (79 ± 5 S cm^{-1}) and Seebeck coefficient (16 ± 1 μV K^{-1}). This novel material has shown sensitivity to different stimuli including strain, as well as ambient temperature and/or air flow.

4. Experimental Section

PEDOT:PSS Clevios PH1000 (from Heraeus GmbH) was freeze dried (using a Benchtop Pro with Omnitronics from SP Scientific), then dispersed in anhydrous DMSO > 99.9% (from Sigma Aldrich) by homogenisation (Heidolph SilentCrusher M set at 500 rpm for 5 min) followed by probe sonication (Sonics VibraCell, amplitude 35%, 1 s on and 1 s off, for 20 min), making up a dispersion with 1 wt% solid content. This process could not be reproduced as efficiently if the PEDOT:PSS was dried by applying heat to the solution, which leads to a compacted dry material. On redispersing with DMSO, a nonhomogeneous casting solution was formed, as compared to the ones using high surface area foam (Section S15A, Supporting Information).

Spandex yarn (Lycra Invista) (Section S15B, Supporting Information) was also dispersed in anhydrous DMSO by stirring at 80 °C for 12 h, to afford a dispersion with 1 wt% solid content.

Both Lycra and PEDOT:PSS dispersions were mixed together at different proportions to make up blends of 1 wt% load, with Lycra content varying from 0% to 100% (Section 15C, Supporting Information). All mixtures were magnetically stirred for a further 24 h at room temperature, drop cast and dried at least ten consecutive times on precleaned glass slides, using an oven set at 80 °C. Films were then mechanically removed from the glass substrate.

The drying temperature was chosen on the basis of thermal gravimetric analysis results using a TA Instruments Q500 Thermogravimetric Analyzer, flushed with air (60 mL min^{-1}), shown in Section S16 in the Supporting Information, with further consideration to the effect of different casting temperatures on the morphology and electrical conductivity (Section S1, Supporting Information).

Mechanical tests were performed using a quasi-static tensile tester (Instron 5566, with a rate of 0.5% per minute, then 10% per minute for 90 wt% Lycra blends after the first 5% strain, in this way to control the timing of the test). Films were prepared as described above, then cut at ≈50 mm × 5 mm surface area. The results for % strain at break and elastic modulus were averaged out of 6 to 10 individual samples, whereas the presented curves were selected from representative results for each composition.

Fourier-transform infrared spectroscopy (FTIR) spectrum of solution blends were recorded using a Bruker Tensor 27, with the DMSO signal eliminated from background.

UV–vis spectra of blends were recorded using a Perkin Elmer Lambda35. In this instance, the DMSO is not eliminated from background spectrum.

AFM images were obtained with a Bruker Dimension Icon operating in quantitative nanomechanical analysis mode on samples drop casted a single time, having films with thickness of about 10 μm.

SEM images were taken with a FEI Inspect F equipped with energy dispersive x-ray spectrometry (EDX). Samples were prepared by consecutively drop casted films (about 10%), with thickness of about 100 μm.

X-ray diffraction (XRD) signals recorded with a diffractometer system XPERT-PRO using K-alpha of 1.54 Å.

A home built four point probe (0.25 mm probe space) is used for electrical conductivity measurements on the substrate, at room temperature and ambient atmosphere using an Agilent 6614 System DC power supply integrated with a Keithley 6485 picoammeter, connected to the external probes. The voltage generated when current passes through the sample is then measured (high impedance Keithley 2000 Multimeter) between the two internal probes. For this purpose, films are prepared by single drop cast, with thickens measured using a profilometer (Bruker Dektak Vision 64), and calculated electrical conductivity averaged out of four films from each blend composition, and measured five times at different points within the centre of the film.

A Seebeck System was used for Seebeck measurements at 300 K under nitrogen atmosphere (MMR, SB100 digital Seebeck controller and K20 digital temperature controller), with self-standing films cut to the dimensions required by the instrument (≈1 mm × 5 mm surface area). The averaged result is calculated out of three films made from each blend composition and measured at least ten times each.

The electrical conductivity and Seebeck coefficient were used for calculation of the power factor, based on Equation (1).

For cyclic test, as well as the self-powered strain sensing experiments, films were prepared as described above for mechanical test. These prototype materials were then fitted with copper electrodes on the extremities, at a distance of about 40 mm apart, then padded using carbon conductive tabs (12 mm diameter from Agar Scientific), to avoid the material being pulled from the electrode during stretching. A constant voltage of about 0.5 V was applied during the cyclic tests using an Agilent 6614 System DC power supply, while current variations with strain recorded using a coupled Agilent 34401A 6 ½ digital multimeter. Details of theoretical calculation model for resistance changes during the cycles were explained in Section S9 in the Supporting Information.

For self-powered tests, heat is applied to one side of the device to generate a thermovoltage, by using a silicon heat pad (RS 12V, 7.5W, item 245–556) connected to a power supply (Farnell D30-2 set at 12V). This thermovoltage is recorded using a high impedance voltameter (Keithley 2000 Multimeter) and the current recorded using a Keithley 6485 picoammeter. Variable strain rates were used, depending on the % applied, aimed for controlling the time of test.

Supporting Information

Supporting Information is available from the Wiley Online Library or from the author.

Acknowledgements

The authors are grateful to the EPSRC Doctoral Training Centre in Plastic Electronics (grant number EP/G037515) for funding this project, with additional financial support from European Thermodynamics Ltd. O.F. acknowledges the Royal Society for support in the frame of his University Research Fellowship. N.M.P. acknowledges support from the European Commission H2020 under the Graphene FET Flagship (WP14 "Polymer Composites" No. 696656) and under the FET proactive ("Neurofibres" No. 732344).

Conflict of Interest

The authors declare no conflict of interest.

Keywords

organics thermoelectricity, polymer blends, self-powered, sensors

Received: July 28, 2017
Revised: October 14, 2017
Published online:

[1] R. F. Service, *Science* **2003**, *301*, 909.
[2] M. J. Cima, *Nat. Biotechnol.* **2014**, *32*, 642.
[3] W. Zeng, L. Shu, Q. Li, S. Chen, F. Wang, X. M. Tao, *Adv. Mater.* **2014**, *26*, 5310.
[4] A. Tricoli, N. Nasiri, S. De, *Adv. Funct. Mater.* **2017**, *27*, 1605271.
[5] T. Dias, *Electronic Textiles: Smart Fabrics and Wearable Technology*. Woodhead Publishing, Cambridge, UK **2015**.
[6] Stanford Wearable Electronics Initiative, https://wearable.stanford.edu (accessed: July 2017).
[7] S. Y. Kuang, J. Chen, X. B. Cheng, G. Zhu, Z. L. Wang, *Nano Energy* **2015**, *17*, 10.
[8] M. Ha, J. Park, Y. Lee, H. Ko, *ACS Nano* **2015**, *9*, 3421.
[9] H. Zhang, Y. Yang, Y. Su, J. Chen, C. Hu, Z. Wu, Y. Liu, C. Ping Wong, Y. Bando, Z. L. Wang, *Nano Energy* **2013**, *2*, 693.
[10] Q. Shi, H. Wang, T. Wang, C. Lee, *Nano Energy* **2016**, *30*, 450.
[11] J. Wang, S. Li, F. Yi, Y. Zi, J. Lin, X. Wang, Y. Xu, Z. L. Wang, *Nat. Commun.* **2016**, *7*, 12744.
[12] R. Vyas, V. Lakafosis, H. Lee, G. Shaker, L. Yang, G. Orecchini, A. Traille, M. M. Tentzeris, L. Roselli, *IEEE Sens. J.* **2011**, *11*, 3139.
[13] Y.-K. Fuh, H.-C. Ho, *Nanotechnology* **2016**, *27*, 95401.
[14] N. S. Hudak, G. G. Amatucci, *J. Appl. Phys.* **2008**, *103*, 101301.
[15] A. R. M. Siddique, S. Mahmud, B. Van Heyst, *Renewable Sustainable Energy Rev.* **2017**, *73*, 730.
[16] E. A. Mondarte, V. Copa, A. Tuico, C. J. Vergara, E. Estacio, A. Salvador, A. Somintac, *Mater. Sci. Semicond. Process.* **2016**, *45*, 27.
[17] Y. Yang, Z. H. Lin, T. Hou, F. Zhang, Z. L. Wang, *Nano Res.* **2012**, *5*, 888.
[18] J. J. Kuchle, N. D. Love, *Measurement: J. Int. Meas. Confed.* **2014**, *47*, 26.
[19] L. Xie, M. Cai, *IEEE Pervasive Comput.* **2014**, *13*, 42.
[20] J. Zhong, Q. Zhong, Q. Hu, N. Wu, W. Li, B. Wang, B. Hu, J. Zhou, *Adv. Funct. Mater.* **2015**, *25*, 1798.
[21] A. Dewan, S. U. Ay, M. N. Karim, H. Beyenal, *J. Power Sources* **2014**, *245*, 129.
[22] B. Sümer, E. K. San, K. Sancakdar, *Procedia Eng.* **2016**, *168*, 63.
[23] N. N. Aung, E. Crowe, X. Liu, *ISA Trans.* **2015**, *55*, 188.
[24] I. Korhonen, R. Lankinen, *Measurement: J. Int. Meas. Confed.* **2014**, *58*, 241.
[25] C. Wang, K. Zhao, Q. Guo, Z. Li, *IET Circuits, Devices Syst.* **2016**, *10*, 147.
[26] V. Leonov, P. Fiorini, T. Torfs, R. Vullers, C. Van Hoof, *Microelectronics Journal* **2011**, *42*, 579.
[27] V. Leonov, T. Torfs, P. Fiorini, C. Van Hoof, *IEEE Sens. J.* **2007**, *7*, 650.
[28] S. Dalola, M. Ferrari, V. Ferrari, M. Guizzetti, D. Marioli, A. Taroni, *IEEE Trans. Instrum. Meas.* **2009**, *58*, 99.
[29] D. Davila, A. Tarancon, C. Calaza, M. Salleras, M. Fernandez-Reglez, A. San Paulo, L. Fonseca, *Nano Energy* **2012**, *1*, 812.
[30] M. Guan, K. Wang, D. Xu, W.-H. Liao, *Energy Convers. Manage.* **2017**, *138*, 30.
[31] Y. Shi, Y. Wang, Y. Deng, H. Gao, Z. Lin, W. Zhu, H. Ye, *Energy Convers. Manage.* **2014**, *80*, 110.
[32] P. J. Taroni, I. Hoces, N. Stingelin, M. Heeney, E. Bilotti, *Isr. J. Chem.* **2014**, *54*, 534.
[33] O. Bubnova, X. Crispin, *Energy Environ. Sci.* **2012**, *5*, 9345.
[34] N. Dubey, M. Leclerc, *J. Polym. Sci., Part B: Polym. Phys.* **2011**, *49*, 467.
[35] G. Kim, L. Shao, K. Zhang, K. Pipe, *Nat. Mater.* **2013**, *12*, 719.
[36] H. Julian Goldsmid, *J. Electron. Mater.* **2017**, *46*, 2599.
[37] T. J. Seebeck, *Abh. Akad. Wiss.* **1822**, *289*.
[38] G. J. Snyder, E. S. Toberer, *Nat. Mater.* **2008**, *7*, 105.
[39] C. Cho, K. L. Wallace, P. Tzeng, J. H. Hsu, C. Yu, J. C. Grunlan, *Adv. Energy Mater.* **2016**, *6*, 1502168.
[40] C. Cho, B. Stevens, J. H. Hsu, R. Bureau, D. A. Hagen, O. Regev, C. Yh, J. C. Grunlan, *Adv. Mater.* **2015**, *27*, 2996.
[41] C. Bounioux, P. Diaz-Chao, M. Campoy-Quiles, M. S. Martin-González, A. R. Goñi, R. Yerushalmi-Rozene, C. Müller, *Energy Environ. Sci.* **2013**, *6*, 918.
[42] B. Dörling, J. D. Ryan, J. D. Craddock, A. Sorrentino, A. El Basaty, A. Gomez, M. Garriga, E. Pereiro, J. E. Anthony, M. C. Weisenberger, A. R. Goñi, C. Müller, M. Campoy-Quiles, *Adv. Mater.* **2016**, *28*, 2782.
[43] A. M. Nardes, M. Kemerink, R. A. J. Janssen, J. A. M. Bastiaansen, N. M. M. Kiggen, B. M. W. Langeveld, A. J. J. M. van Breemen, M. M. de Kok, *Adv. Mater.* **2007**, *19*, 1196.
[44] K.-C. Chang, M.-S. Jeng, C.-C. Yang, Y.-W. Chou, S.-K. Wu, M. A. Thomas, Y.-C. Peng, *J. Electron. Mater.* **2009**, *38*, 1182.
[45] C. Liu, B. Lu, J. Yan, J. Xu, R. Yue, Z. Zhu, S. Zhou, X. Hu, Z. Zhang, P. Chen, *Synth. Met.* **2010**, *160*, 2481.
[46] T.-C. Tsai, H.-C. Chang, C.-H. Chen, W.-T. Whang, *Org. Electron.* **2011**, *12*, 2159.
[47] A. M. Nardes, R. a. J. Janssen, M. Kemerink, *Adv. Funct. Mater.* **2008**, *18*, 865.
[48] X. Crispin, S. Marciniak, W. Osikowicz, G. Zotti, A. W. D. van Der Gon, F. Louwt, M. Fahlman, L. Groenendaal, F. De Schryver, W. R. Salaneck, *J. Polym. Sci., Part B: Polym. Phys.* **2003**, *41*, 2561.
[49] O. Bubnova, M. Berggren, X. Crispin, *J. Am. Chem. Soc.* **2012**, *134*, 16456.
[50] O. Bubnova, Z. U. Khan, A. Malti, S. Braun, M. Fahlman, M. Berggren, X. Crispin, *Nat. Mater.* **2011**, *10*, 429.
[51] T. Park, C. Park, B. Kim, H. Shin, E. Kim, *Energy Environ. Sci.* **2013**, *6*, 788.
[52] T. Murakami, Y. Mori, H. Okuzaki, *Trans. Mater. Res. Soc. Jpn.* **2011**, *168*, 165.
[53] J. Kim, J. Jung, D. Lee, J. Joo, *Synth. Met.* **2002**, *126*, 311.
[54] F. Zhang, Y. Zang, D. Huang, C. Di, D. Zhu, *Nat. Commun.* **2015**, *6*, 8356.
[55] Q. Wei, M. Mukaida, Y. Naitoh, T. Ishida, *Adv. Mater.* **2013**, *25*, 2831.
[56] H. J. Qi, M. C. Boyce, *J. Mech. Phys. Solids* **2004**, *52*, 2187.

ADVANCED FUNCTIONAL MATERIALS

Supporting Information

for *Adv. Funct. Mater.,* DOI: 10.1002/adfm.201704285

Toward Stretchable Self-Powered Sensors Based on the Thermoelectric Response of PEDOT:PSS/Polyurethane Blends

*Prospero J. Taroni, Giovanni Santagiuliana, Kening Wan, Philip Calado, Manting Qiu, Han Zhang, Nicola M. Pugno, Matteo Palma, Natalie Stingelin-Stutzman, Martin Heeney, Oliver Fenwick, Mark Baxendale, and Emiliano Bilotti**

Supporting Information

DOI: 10.1002/adfm.201704285
Article type: Full Paper

Title: Towards Self-Powered Strain Sensors Based on the Thermoelectric Response of PEDOT:PSS/Polyurethane Blends.

*Prospero J. Taroni, Giovanni Santagiuliana, Kening Wan, Philip Calado, Manting Qiu, Han Zhang, Matteo Palma, Natalie Stingelin-Stutzman, Martin Heeney, Oliver Fenwick, Mark Baxendale, Emiliano Bilotti**

P.J. Taroni, G. Santagiuliana, K. Wan, Dr. H. Zhang, Dr. O. Fenwick, Dr. E. Bilotti
School of Engineering and Material Sciences, Queen Mary University of London, Mile End Road, E1 4NS, London, UK
E-mail: e.bilotti@qmul.ac.uk
Dr. Mark Baxendale, Manting Qiu
School of Physics and Astronomy, Queen Mary University of London, Mile End Road, London, E1 4NS, UK
Prof. N. Stingelin-Stutzman
School of Materials Sciences, Georgia Tech, 771 Ferst Drive, J. Erskine Love Building, Atlanta, GA 30332-0245
Prof. M. Heeney,
School of Chemistry and Centre of Plastic Electronics, Imperial College London, London SW7 2AZ, UK
P. Calado,
School of Physics, Imperial College London, London SW7 2AZ, UK
Dr Matteo Palma
School of Biological and Chemical Sciences, Joseph Pristley building, Mile End Road, London, E1 4NS

SUPPORTING INFORMATION 1 – The effect of casting temperature

PEDOT:PSS with 50 wt.% Lycra® was used for a comparative analysis of electrical conductivity correlated to morphology, based on the effect of casting temperature, for pristine films, annealed, as well as after ethylene glycol (EG) treatment **(Figure SI-1A)**. After initial electrical measurements for the films casted at temperatures between 50 and 130°C, they were annealed in an oven set at 130ºC for 1 hour than measured again for electrical conductivity. The same films are then immersed in an EG bath for 2 hours, then dried in an oven set at 130ºC, and measured a final time for electrical conductivity. The effect of annealing

temperature is apparently not as significant when compared to the effect of EG treatment, which leads to consistently enhanced electrical conductivity for all the casting temperatures studied.

The increased casting temperature has a significant but detrimental effect, explained in terms of morphological structure. It seems that partial phase segregation between components of the composite has occurred at higher casting temperatures (**Figure SI-1B** and **C**). The Lycra® component, as a non-conductive material may have served as barrier for charge transport on a more segregated film microstructure.

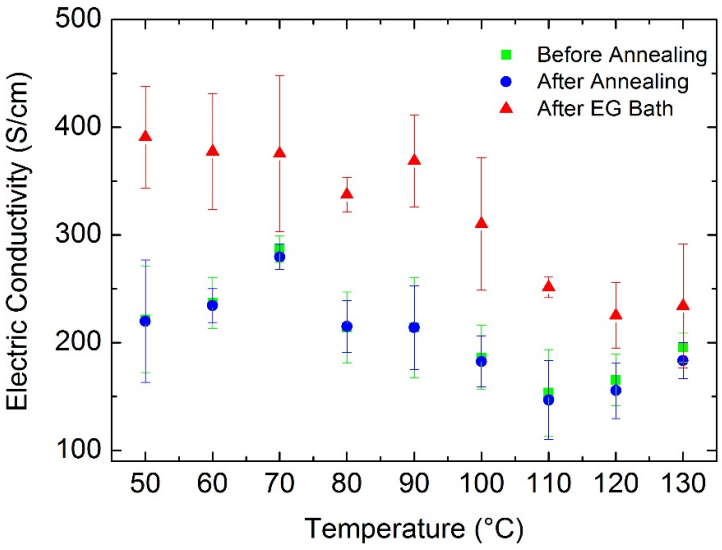

(a)

(b) (c)

Figure SI-1: (a) Graph of electrical conductivity *vs.* casting temperature, before and after annealing, also after EG treatment for 50 wt.% Lycra® composite, (b) photographic image of film casted at 50°C and (c) 130°C.

SUPPORTING INFORMATION 2 – The best mechanical properties

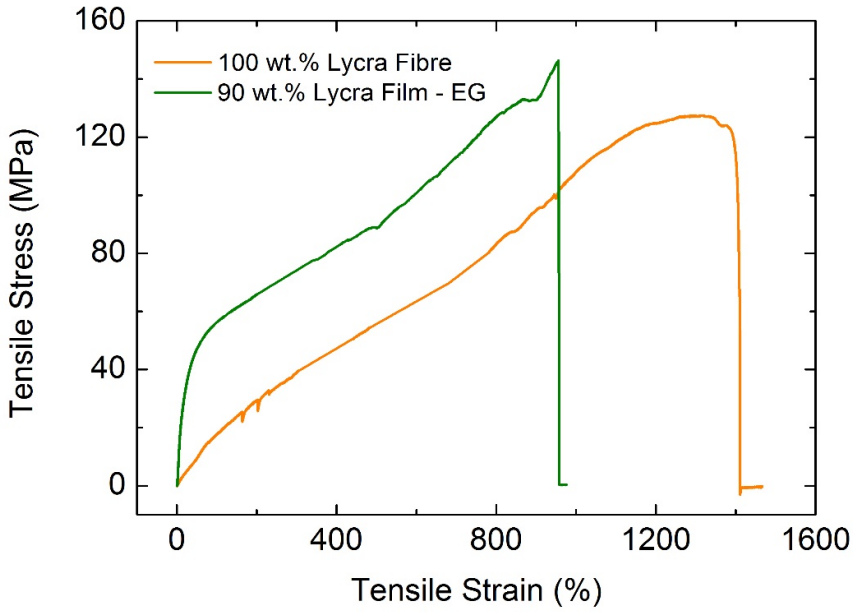

(a)

(b)

Figure SI-6: (a) Best result for 90 wt.% Lycra® after EG bath, close to a representative result for the original yarn. The values for this blend ranged from 580 to 950 %, with an average of ~700 ± 150% and (b) images of film at no extension and high extension.

SUPPORTING INFORMATION 3 – Ethylene glycol (EG) treatment

Films with proportions ranging from 0% to 90% Lycra® were measured for electrical conductivity, then immersed in an EG bath for 2 hours, dried and measured again for electric conductivity. The results show improvment in the electrical conductivity with the EG treatment, presented in Figure **SI-3**A and tabulated in **SI-3B**. There seems to be a trend of increased % effect at higher concentrations of Lycra®.

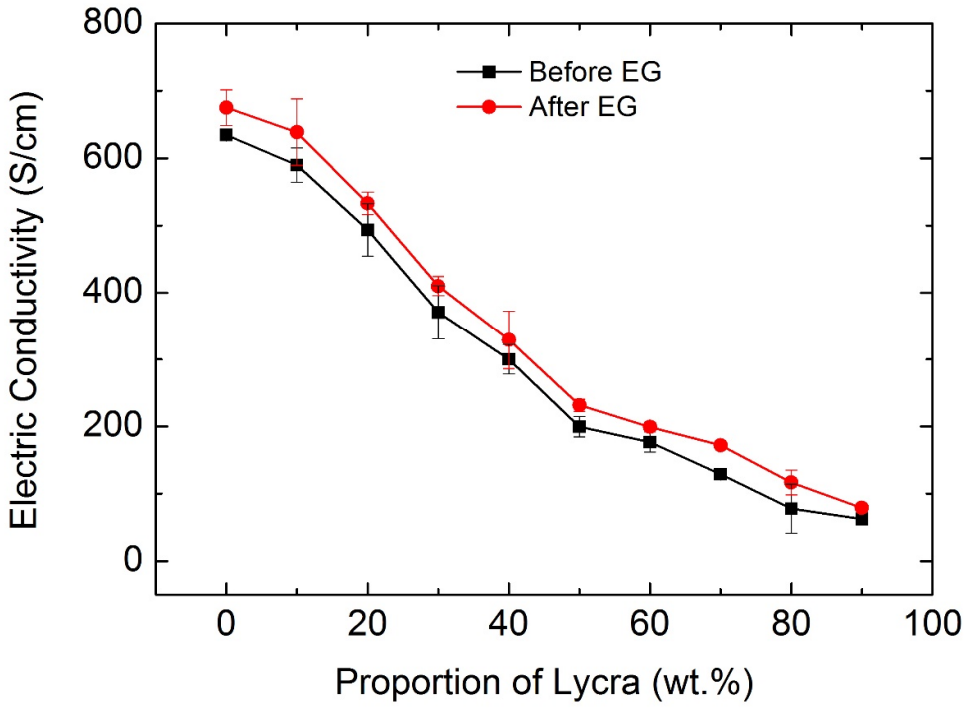

Average electrical conductivity										
Proportion of Lycra®	0	10	20	30	40	50	60	70	80	90
Before EG treatment	635 ±8	590 ±25	490 ±40	370 ±40	300 ±22	200 ±15	177 ±15	129 ±6	80 ±40	62 ±4
After EG treatment	675 ±27	640 ±50	533 ±17	410 ±14	330 ±40	232 ±9	199 ±7	172 ±3	117 ±19	79 ±5

Figure SI-3: (a) Scatter of electrical conductivity *vs*. proportion of Lycra®, before and after EG bath with (b) tabulated results.

SUPPORTING INFORMATION 4 – XRD of PEDOT:PSS before and after EG bath

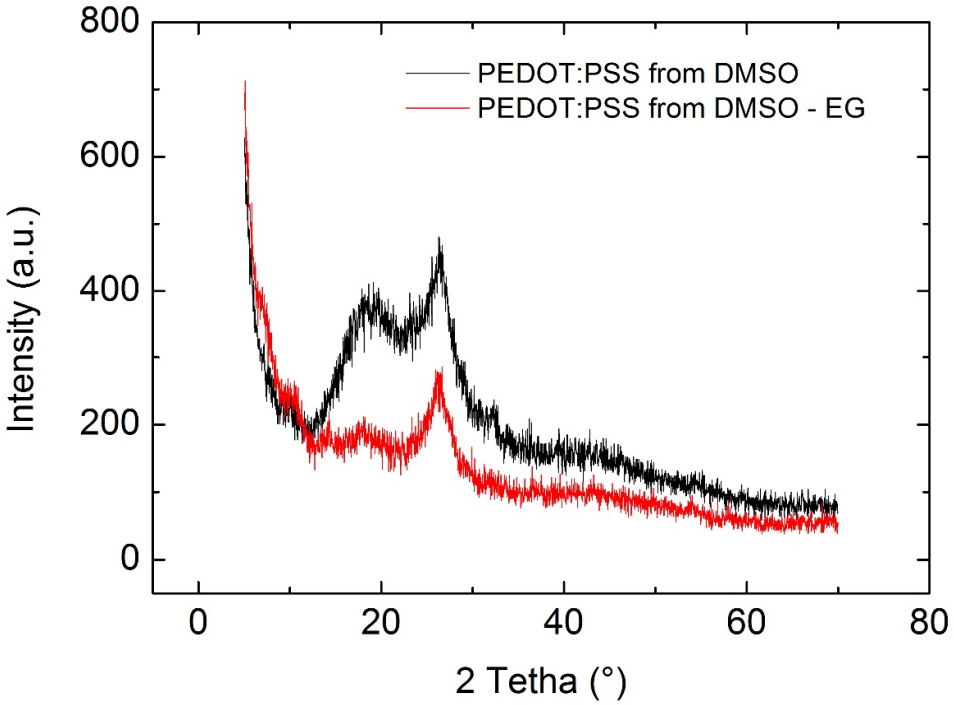

Figure SI-4: XRD (K-alpha of 1.54Å) for PEDOT:PSS cast from DMSO, before and after EG bath, showing reduction of PSS peak at around 18°, previously identified by other sources,[1] whereas the peak at around 26° assigned to PEDOT retained a similar shape. In this way, elimination of PSS with EG treatment can be deduced, whereas the crystallisation of PEDOT with agglomeration of particles is not apparent on this XRD spectrum.

SUPPORTING INFORMATION 5 – Seebeck coefficient of PEDOT:PSS Clevios PH1000, before and after EG bath, at different testing temperatures.

Temperature (K)	Seebeck (uV/K) before EG	StDev	Seebeck (uV/K) after EG	StDev
300	**16.0**	1.37	**15.9**	2.20
350	**16.3**	2.11	**16.5**	2.30
400	**16.8**	2.92	**17.0**	2.90

Table SI-5: Seebeck coefficient of PEDOT:PSS Clevios PH1000 at different temperatures, before and after EG treatment, averaged out of 6 samples measured 10 times at each temperature. It is evident the Seebeck coefficient is not affected by EG treatment.

SUPPORTING INFORMATION 6 – UV/Vis and FTIR

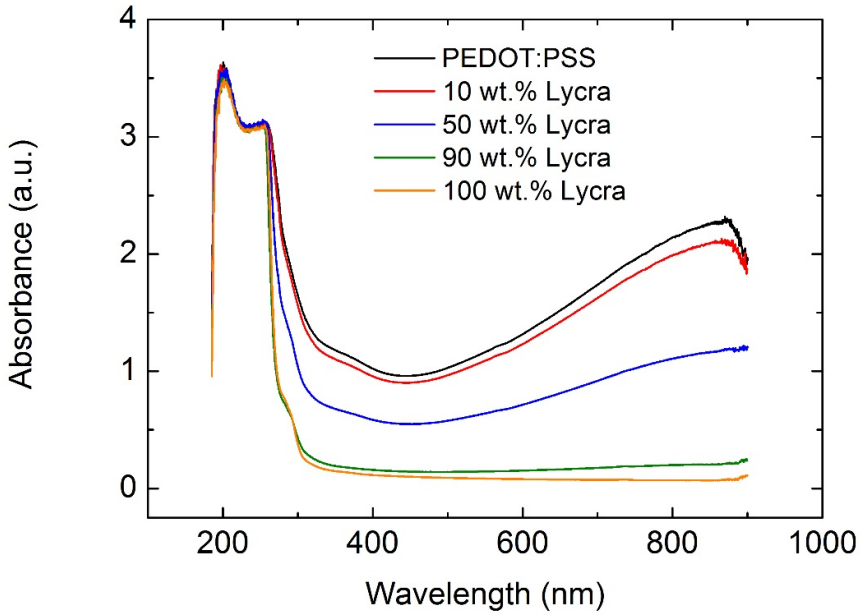

(a)

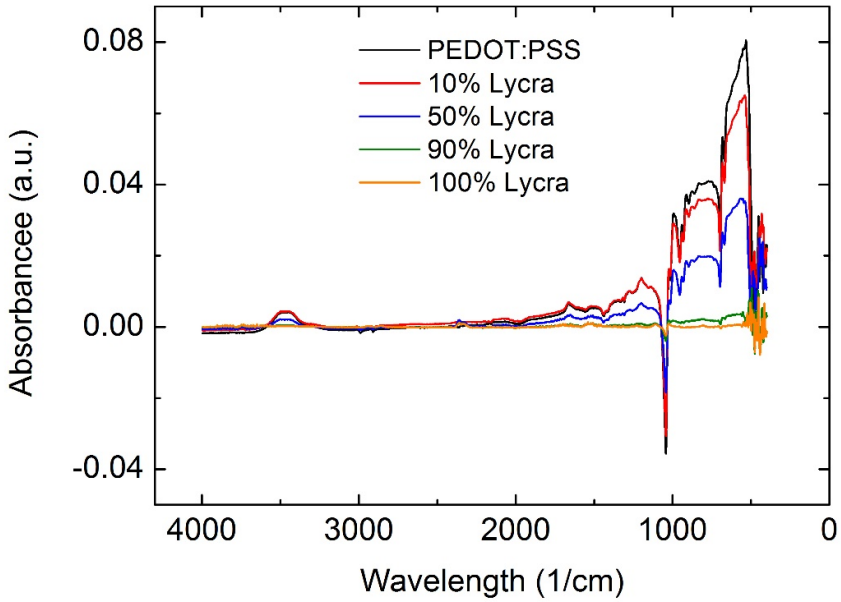

(b)

Figure SI-6: (a) UV/Vis and (b) FTIR of different PEDOT:PSS blends, showing the dilution effect, interpreted from the progressive change in intensities of absorption on the spectrum of the different blends, as the proportions change from one component material to another. No new functional groups are apparent in the FTIR of composites when compared to the pure PEDOT:PSS and Lycra®.

SUPPORTING INFORMATION 7 – Other AFM images

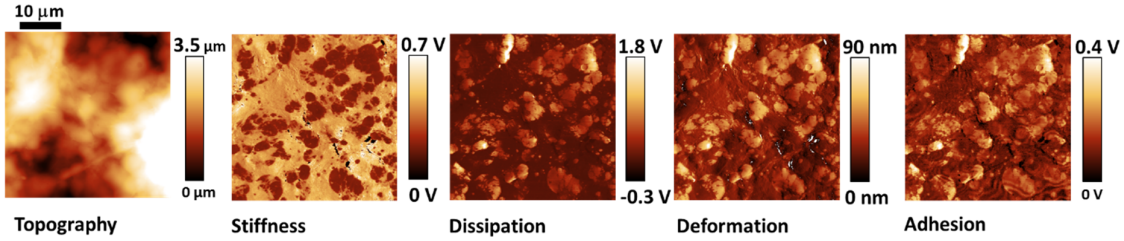

Figure SI-7 (a): Full nanomechanical data for a composite film containing 60% Lycra®, cast at 80°C and after EG treatment. The two phases are not visible in the topography image, but we identify the region with low elastic modulus as belonging to a Lycra®-rich phase, which deforms more than the PEDO:PSS phase under the force of the AFM tip, also showing more adhesion and more dissipation.

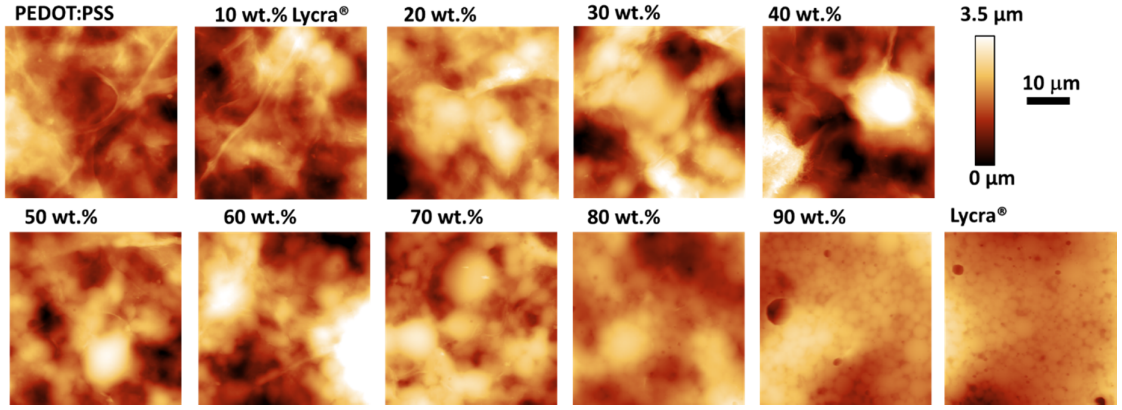

Figure SI-7 (b): AFM topography images of PEDOT:PSS and Lycra® composites at different blend proportions (0% to 100% Lycra®, 10% increment), after EG treatment.

SUPPORTING INFORMATION 8 – SEM before and after EG bath

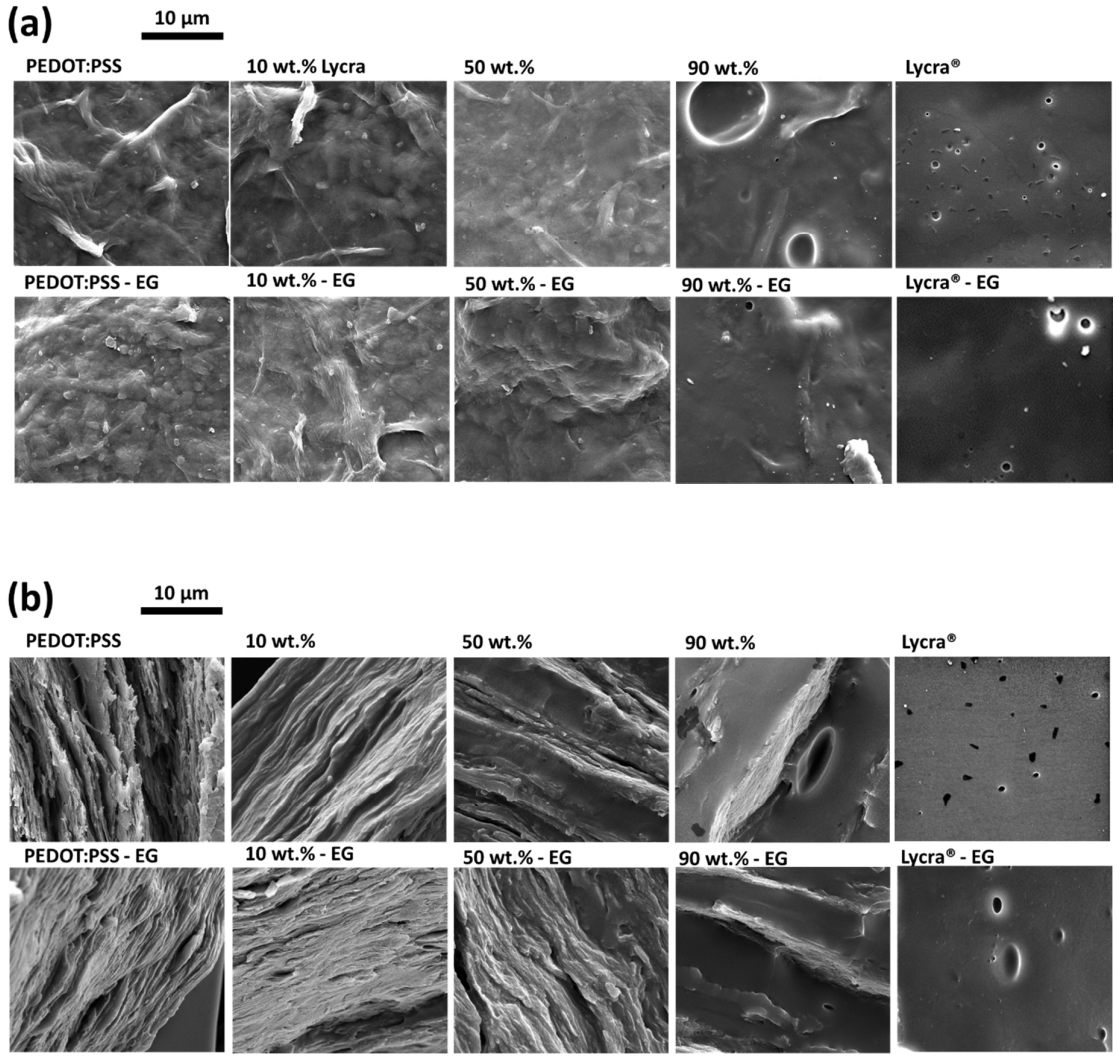

Figure SI-8: (a) Top surface and (b) cross-section SEM images of PEDOT:PSS and Lycra® composites at different proportions (0%, 10%, 50%, 90% and 100% Lycra® (from left to right), before and after EG bath (top and bottom, respectively).

SUPPORTING INFORMATION 9 - Modelling method and preliminary results.

The theroretical effect of geometric factors on resistance of the composite film (R_T) is calculated using equation 1:

$$R_T = \rho_0 \times \frac{L}{A} \quad [1]$$

where the initial resistivity (ρ_0) is calculated using initial values measured for resistance (R_0), initial cross-sectional area (A_0) and initial length (L_0), shown by equation 2:

$$\rho_0 = R_0 \times \frac{A_0}{L_0} \quad [2]$$

The length (L) is recorded by the universal tensile tester at a given strain.

The cross sectional area (A) is calculated using the equation 3:

$$A = W \times T \quad [3]$$

The width (W) and thickness (T) are calculated from the initial width and thickness, W_0 and T_0, using the equations 4 and 5, and a Poisson ratio of 0.5 for incompressible materials:[2]

$$W = W_0 \left(1 - \left(0.5 \times \frac{Extension}{L_0}\right)\right) \quad [4]$$

$$T = T_0 \left(1 - \left(0.5 \times \frac{Extension}{L_0}\right)\right) \quad [5]$$

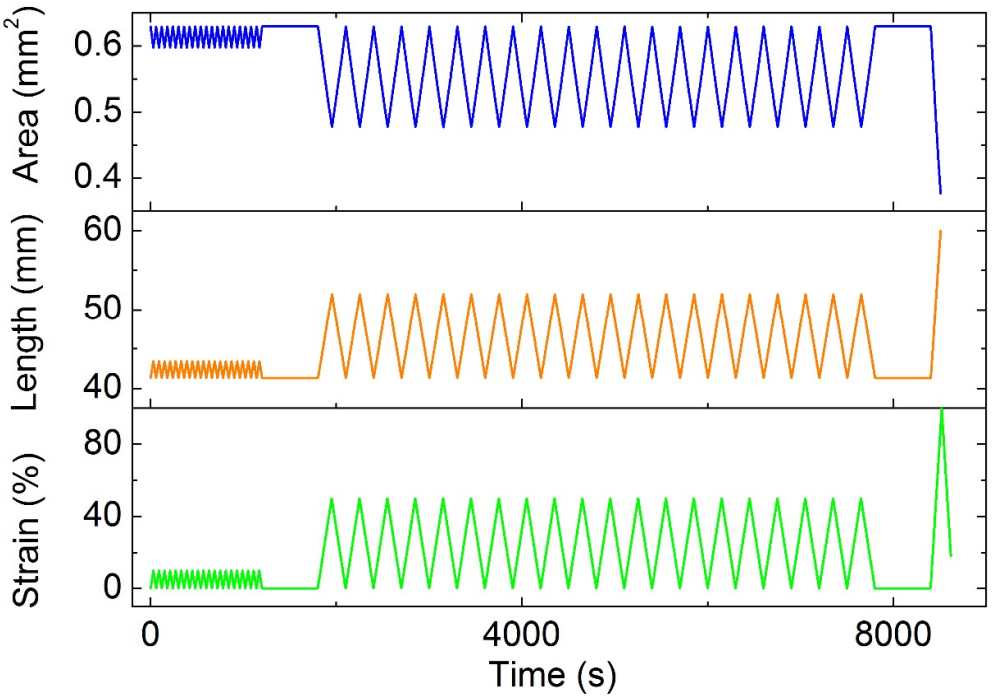

Figure SI-9: Results showing calculated area, recorded length (L), for cyclic signals recorded while applying up to 10% and 50% strains.

SUPPORTING INFORMATION 10 - Modelling method at higher strain %

The calculated values of resistance (R_T) shown in **Figure SI-10** are lower than the measured values, for strains greater or equal to 80%, indicating that, if the Poisson ratio has not changed under plastic deformation, geometric factors does not account for all the variations in resistance, and therefore conductivity changes may be involved with higher strains. Once the sample was extended by 80% of its initial length, the measured resistance is close to calculated, but it does not recover, indicating the onset of plastic deformation. At higher strains, 150%, 250% and 300%, this deformation is accentuated, indicating further changes in the material conductivity.

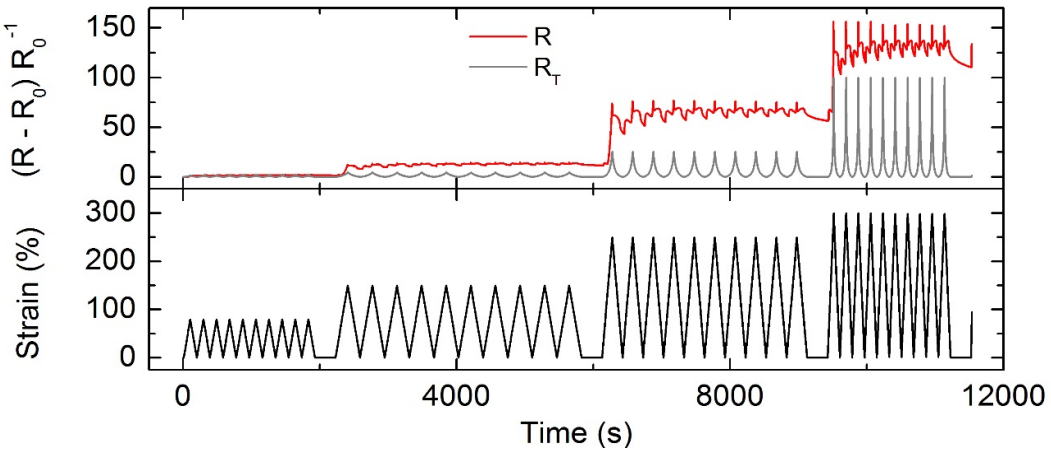

Figure SI-10: $(R-R_0)\ R_0^{-1}$ signal generated by the PEDOT:PSS blend with 90% Latex® after EG bath, when 80% strain is applied, followed by 150%, 250 and 300% (Gauge factor ~ 1.9, 9.4, 29.6 and 47.7, respectively).

SUPPORTING INFORMATION 11

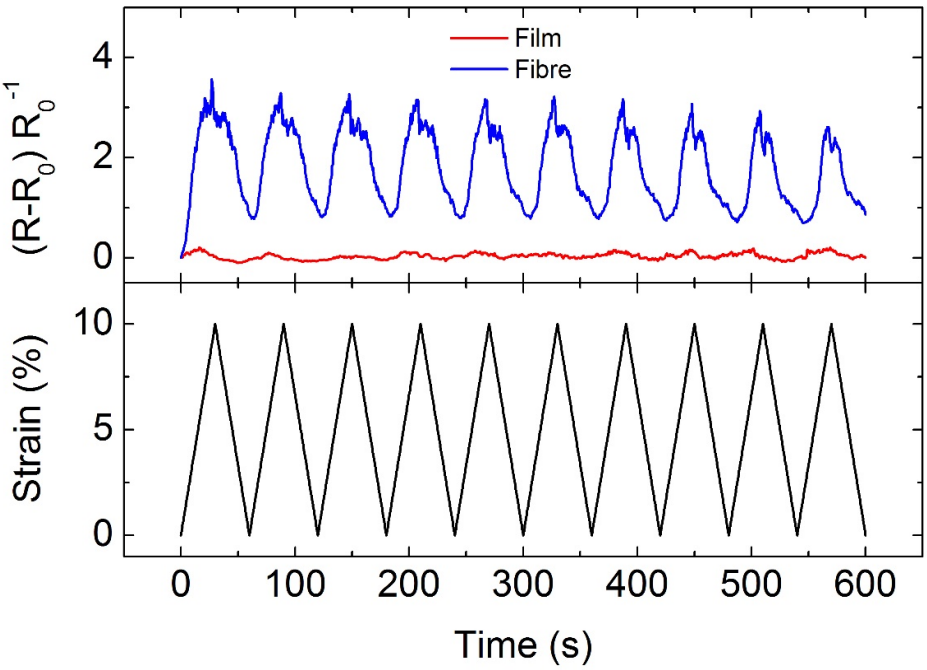

(a) **(b)**

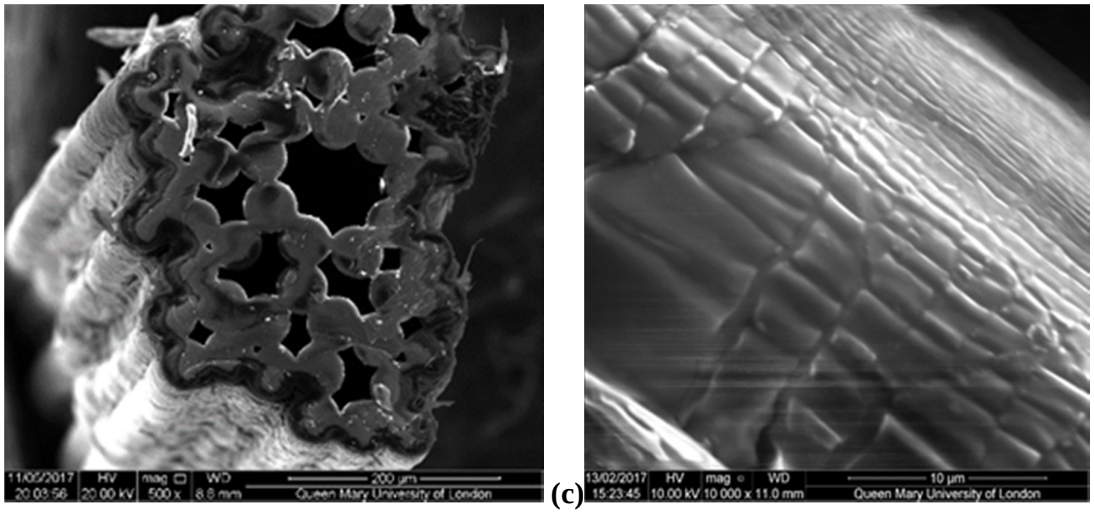

(c)

igure SI-11 (a) Measured (R-R_0) R_0^{-1} as a function of strain for fibre coated with PEDOT:PSS (blue), and film of 90 wt.% Lycra® (red), (b) the cross-section SEM image of coated fibre, and (c) the stretched surface of a fibre coated with PEDOT:PSS.

SUPPORTING INFORMATION 12 – Assessment of thermovoltage (V_{oc}) and strain sensitivity.

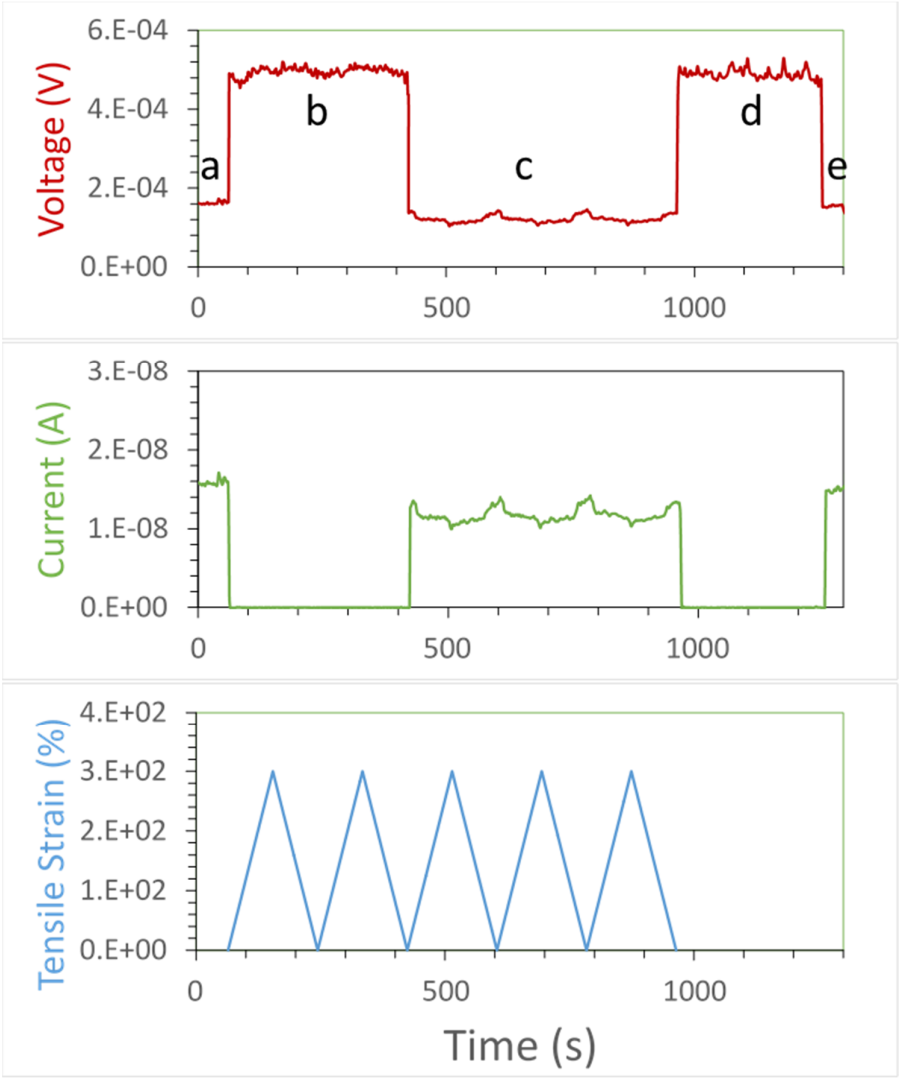

Figure SI-12: Voltage, current, and tensile strain showing (a) 10 KΩ load and no strain, (b) open circuit with 2 cycles of 300% strain (full thermovoltage and no current), (c) 10 KΩ load with 3 cycles of 300% strain (reduced thermoevoltage with good sensitivity to strain), (d) open circuit with no strain, and (e) 10 KΩ load and no strain.

SUPPORTING INFORMATION 13 – Self powered sensors with sensitivity to other stimuli (environmentaal effect – ambient temperature and air draft).

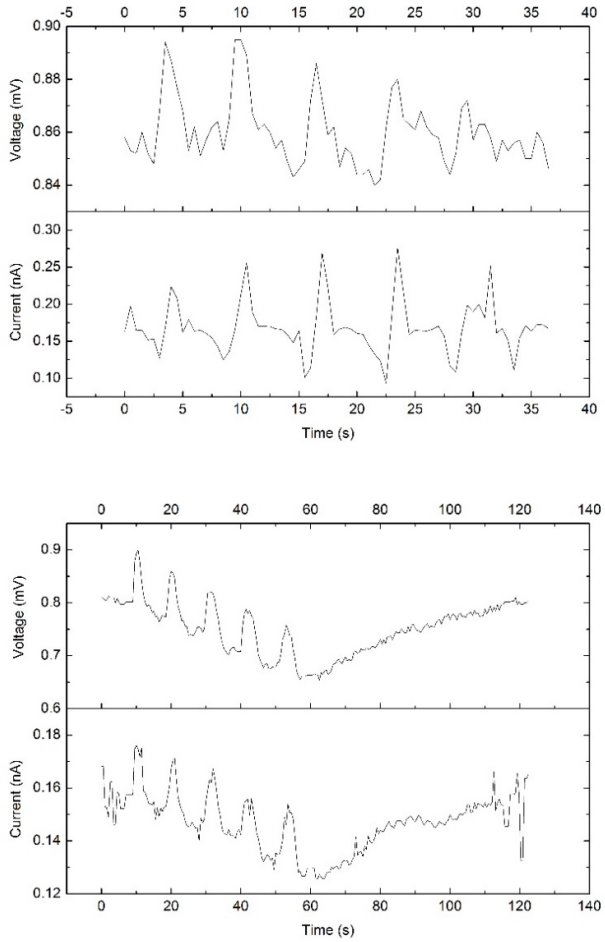

Figure SI-13: It has been established that the noise in the data was not measurement noise or mechanical instability, it came from environmental fluctuations. This was confirmed by observing a voltage/current increase by breathing towards the PEDOT/Lycra® device (Video SI-13A). To eliminate the effect of humidity, the samples were also investigated with consecutive blows of an air dryer (Video SI-13B).

SUPPORTING INFORMATION 14 – Sensor power output.

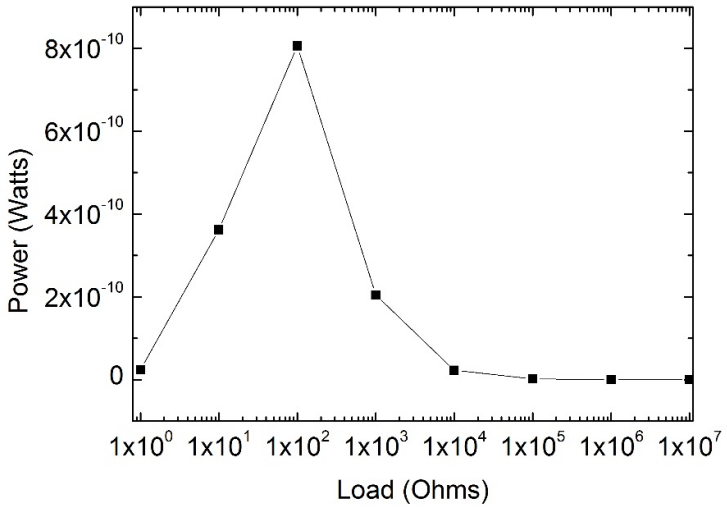

Figure SI-14: Power output of a film containing 10 wt.% PEDOT:PSS and 90 wt.% Lycra®, for a ΔT of 30 ˚C, as a function of the load resistance, achieving a maximum for a resistance matching the internal sample resistance.

SUPPORTING INFORMATION 15 – Materials

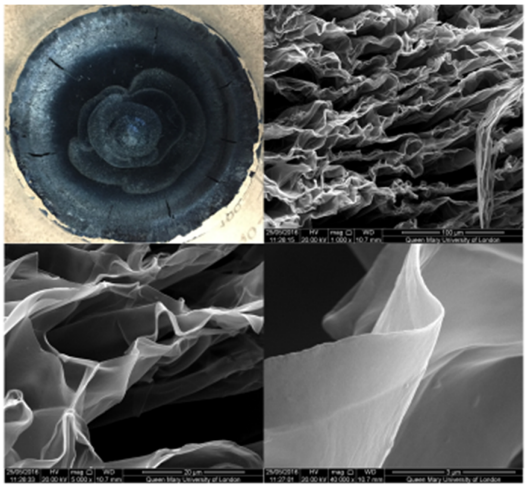

SI-15A – Photograph and SEM images of freeze dried PEDOT:PSS anhydrous foam, showing high surface area structure.

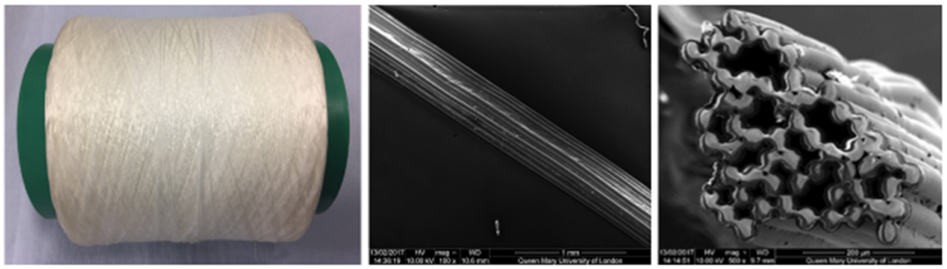

SI-15B – Photograph and SEM images (surface and cross section) of Lycra® yarn.

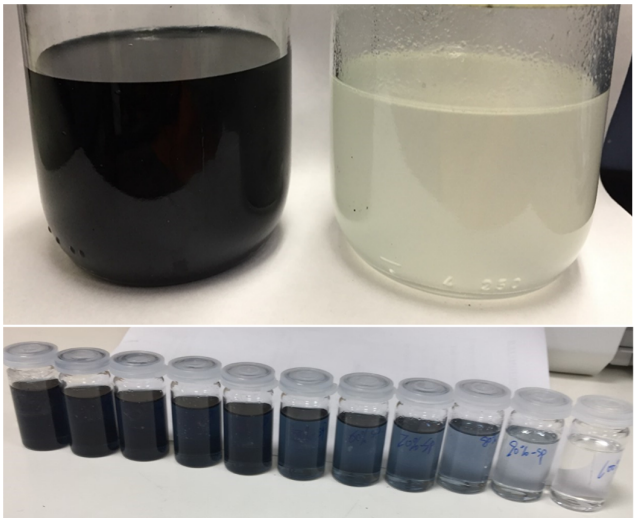

SI-15C – Photographs of casting solutions (1 wt.% solid content) with different Lycra® content (0 to 100 wt.%).

SUPPORTING INFORMATION 16 – Thermal Gravimetric Analysis (TGA)

The individual components as well as the 50% PEDOT:PSS/ Lycra® composite have also been analysed by TGA, to gain an insight on the best processing temperature. The initial weight loss below 200°C for all samples could be attributed to desorption of residual DMSO solvent. For pure PEDOT:PSS sample (0% Lycra®) the weight loss was slightly higher, in this range, possibly due to added desorption of moisture, which is expected compared to the elastomer, a hydrophobic compound. The pure PEDOT:PSS has shown two main degradation peaks, one attributed to PSS [3], between 230°C to 380°C, and another peak attributed to PEDOT [3], between 380°C to 490°C. Pure Lycra® have shown three degradation peaks, one between 250°C to 360°C, another between 360°C and 460°C and the last peak between 460°C and 580°C. These different degradations have not been assigned but may be attributed to the different sections of the Lycra® molecule, which is a copolymer composed of soft and hard segments.[2] The 50% composite behaved within the above ranges and all the samples have been concluded safe to be processed at temperatures below 150 °C.

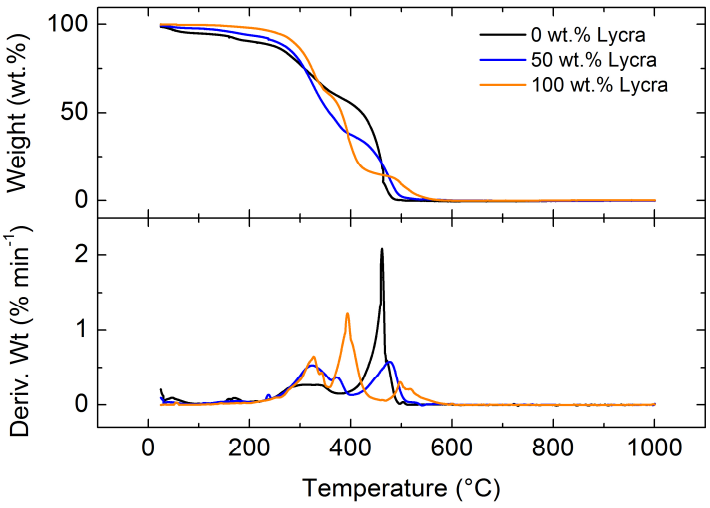

Figure SI-16: Thermal Gravimetric Analysis of PEDOT:PSS, Lycra® and their 50% composite showing (a) % weight vs. temperature and (b) derivative weigh.

References:

1. Zhang, X., Chang, D. & Luo, Y. Conducting polymer aerogels from supercritical CO 2 drying PEDOT-PSS hydrogels. 5080–5085 (2010). doi:10.1039/c0jm00050g

2. Qi, H. J. & Boyce, M. C. Stress-Strain Behavior of Thermoplastic Polyurethane. 1–51 (2004).

3. Takahashi, T., Ishihara, M. & Okuzaki, H. Poly(3,4-ethylenedioxythiophene)/poly(4-styrenesulfonate) microfibers. *Synth. Met.* **152,** 73–76 (2005).